

**Title: Evaluation of PET Brain Radioligands for Imaging Pancreatic  $\beta$ -Cell Mass: Potential Utility of  $^{11}\text{C}$ -(+)-PHNO**

**Running Title:** Imaging  $\beta$ -Cell Mass with  $^{11}\text{C}$ -(+)-PHNO

**Authors:** Jason Bini<sup>1,2</sup>, Mika Naganawa<sup>1</sup>, Nabeel Nabulsi<sup>1</sup>, Yiyun Huang<sup>1</sup>, Jim Ropchan<sup>1</sup>, Keunpoong Lim<sup>1</sup>, Soheila Najafzadeh<sup>1</sup>, Kevan C. Herold<sup>3</sup>, Gary W. Cline<sup>3</sup>, Richard E. Carson<sup>1,2</sup>

**Affiliations:** <sup>1</sup>PET Center, Yale University School of Medicine, New Haven, CT; <sup>2</sup>Department of Biomedical Engineering, Yale University, New Haven, CT; <sup>3</sup>Department of Immunobiology and Internal Medicine, Yale University School of Medicine, New Haven, CT

**Disclaimer:** None

**First Author and Corresponding Author:**

Jason Bini  
801 Howard Avenue  
PO Box 208048  
New Haven, CT  
Phone: 203-737-9738  
Fax: 203-785-3107

**Word Count:** 5000

**Keywords:** Diabetes, Pancreas,  $\beta$ -cell mass, PHNO, PET

## **ABSTRACT**

Type 1 diabetes mellitus (T1DM) is characterized by a loss of beta cells in the islets of Langerhans of the pancreas and subsequent deficient insulin secretion in response to hyperglycemia. Development of an *in vivo* test to measure β-cell mass (BCM) would greatly enhance the ability to track diabetes therapies. β-cells and neurological tissues have common cellular receptors and transporters, therefore, we screened brain radioligands for their ability to identify β-cells.

## **Methods**

We examined a β-cell gene atlas for endocrine pancreas receptor targets and cross-referenced these targets with brain radioligands that were available at our institution. Twelve healthy control (HC) subjects and two T1DM subjects underwent dynamic positron emission tomography/computed tomography (PET/CT) scans with six tracers.

## **Results**

The D<sub>2</sub>/D<sub>3</sub>-receptor agonist radioligand <sup>11</sup>C-(+)-4-propyl-9-hydroxynaphthoxazine (PHNO) was the only radioligand to demonstrate sustained uptake in the pancreas with high contrast versus abdominal organs such as the kidneys, liver, and spleen, based on the first 30 min of data. Mean standardized uptake value (SUV) from 20-30 minutes demonstrated high uptake of <sup>11</sup>C-(+)-PHNO in HCs (SUV:13.8) with a 71% reduction in a T1DM subject with undetectable levels of C-peptide (SUV:4.0) and a 20% reduction in a T1DM subject with fasting C-peptide level of 0.38 ng/mL (SUV:11.0). SUV in abdominal organs outside the pancreas did not show measurable differences between the control and T1DM subjects, suggesting that the changes in SUV of <sup>11</sup>C-(+)-PHNO may be specific to changes in the pancreas between HCs and T1DM subjects. Using D<sub>3</sub>- and D<sub>2</sub>-antagonists, in non-human primates (NHP), specific pancreatic binding (SUVR-1) of <sup>11</sup>C-PHNO was reduced by 57% and 38%, respectively.

## **Conclusion**

<sup>11</sup>C-(+)-PHNO is a potential marker of BCM with 2:1 binding of D<sub>3</sub>-receptors over D<sub>2</sub>-receptors. Further *in vitro* and *in vivo* studies to establish D<sub>2</sub>/D<sub>3</sub>-receptor specificity to β-cells is warranted to characterize <sup>11</sup>C-(+)-PHNO as a candidate for clinical measurement of BCM in HC and diabetic subjects.

## INTRODUCTION

T1DM is characterized by a loss of  $\beta$ -cells in the islets of Langerhans of the pancreas and the subsequent inability to secrete insulin in response to hyperglycemia(1). Current understanding of how the loss of BCM contributes to loss of function has been largely determined from post-mortem analysis. In the absence of clinically-validated methods to measure BCM *in vivo*, functional studies have been used as a surrogate. However, functional studies, such as C-peptide levels, a measure of endogenous insulin production by  $\beta$ -cells, can be affected by factors including fatty acids, insulin resistance, and even glucose itself. Current tests, such as the oral glucose tolerance test, may not accurately correlate with BCM due to  $\beta$ -cells that are not responsive to stimuli but may still be viable and responsive to treatment. In addition, the sensitivity of  $\beta$ -cells to provocative stimuli may change during different stages of diabetes(2–4). Therefore, development of techniques to measure BCM *in vivo* would greatly enhance the ability to simultaneously track changes in BCM and function, and to evaluate the efficacy and mechanisms of therapies to preserve or restore insulin secretion(5). Several modalities have been proposed for imaging BCM such as PET, single-photon emission computed tomography, magnetic resonance imaging, and optical methods(6).

Previous PET studies have attempted to measure BCM by targeting receptors specific to the endocrine pancreas(7–16). Two radioligands with promising results were  $^{18}\text{F}$ -FP-(+)-Dihydrotetrabenazine (DTBZ), which targets vesicular monoamine transporter 2 (VMAT2) and colocalizes with insulin secretory vesicles(7–9,11) and  $^{11}\text{C}$ -5-hydroxytryptophan (5HTP), a precursor of serotonin present in  $\beta$ -cells that may be involved in insulin secretion(10,12,14). For  $^{18}\text{F}$ -FP-(+)-DTBZ, binding may not be entirely specific to  $\beta$ -cells as there is some evidence of binding in polypeptide cells(17). For  $^{11}\text{C}$ -5HTP, despite demonstrating binding in the islets of Langerhans, it is not clear that binding was specific to  $\beta$ -cells and not due to other endocrine cells(10,12,14). Dopamine, co-secreted with insulin, may act as an autocrine signal via its binding to dopamine receptors on the surface of  $\beta$ -cells and thus may be a useful target(18,19).

$\beta$ -cells and neurological tissues have common cellular receptors and transporters, and therefore, we screened other brain radioligands for their ability to identify  $\beta$ -cells. We used a  $\beta$ -cell gene atlas to identify possible endocrine pancreas receptor targets and cross-referenced these targets with PET brain radioligands that were available at our institution. Existing radioligands were then examined for high pancreatic uptake and high contrast to neighboring organs to determine which radioligands warranted further study. Those radioligands that exhibited such features were tested in T1DM subjects and NHP.

## MATERIALS AND METHODS

### Subjects

Twelve HC subjects (6M/6F) and two male T1DM subjects were included in the study. The average age and weight was  $33 \pm 9$ y and  $76 \pm 12$ kg, respectively. Diabetes duration, at time of scan, for T1DM subjects was 29yrs (fasting C-peptide undetectable) and 14yrs (fasting C-peptide 0.38ng/mL), all healthy controls were screened to exclude existing diabetes (normal fasting C-peptide range: 0.8-3.1ng/mL). The study was approved by the Yale University Institutional Review Board and Radiation Safety Committees, and all subjects signed a written informed consent.

### $\beta$ -Cell Gene Atlas Screening

We cross-referenced the targets of available radioligands at the Yale PET Center with a  $\beta$ -cell gene atlas to find radioligands that may be useful BCM biomarkers(20). Relative Affymetrix  $\beta$ -cell gene expression is defined on a 0-100 scale with 0-25: no expression; 25-50: low; 50-75: moderate, and 75-100: enriched. All radioligands with a relative expression  $\geq 50$  (moderate or enriched expression) were considered potentially useful.

### Human Imaging

Based on the gene atlas, we chose six radioligands for evaluation. Human PET/CT imaging was performed on a Siemens Biograph mCT-X PET/CT system (Siemens Healthcare). A 30-minute dynamic scan (6x30s, 3x60s, 2x120s, 4x300s) centered on the pancreas was performed followed by a 30-minute

whole-body acquisition (2 passes, 120s per bed position) followed by an additional 60-minute dynamic scan (12x300s) at the level of the pancreas. Injected doses and mass for each radioligand are provided in Table 1. Dynamic scans were reconstructed using an ordered subset expectation maximization-based algorithm with point spread function and time-of-flight correction. Attenuation correction was performed using the CT acquisition. Regions-of-interest (ROIs) were drawn manually on a summed image (0-10min), then eroded to avoid partial volume effects, for pancreas, liver, kidneys and spleen, and time activity curves (TACs) were produced in SUV units. SUV and SUV ratio (SUVR, spleen as reference)(13) were calculated on summed images (20-30 minutes). No respiratory motion correction was performed; a previous study demonstrated an underestimation of only 15±6% in non-corrected scans for <sup>18</sup>F-FP-(+)-DTBZ(21).

### **Non-human Primate Imaging**

NHP studies were performed to evaluate D<sub>2</sub>- and D<sub>3</sub>-specific binding components in the pancreas. A NHP (age:13y; weight:20.9kg) underwent scans on two days, with 2 scans per day: baseline followed by blocking scan with tracer injections separated by four hours. Mean injected doses were 182±1 MBq and mass was 0.64±0.10 µg. The blocking scans began 30 min after an infusion of 1) D<sub>3</sub>-selective antagonist SB277011A (1mg/kg), and 2) D<sub>2</sub>-selective antagonist L-741,626 (1mg/kg). Acquisitions on the mCT-X included a 30-min dynamic scan (6x30s, 3x60s, 2x120s, 4x300s) centered on the pancreas followed by a 4-bed (3 min/bed) whole-body acquisition with three passes from head to thigh (36min total). ROIs were drawn manually on a summed image from 0-10 min for the pancreas and spleen. Mean pancreatic SUV and SUVR (spleen as reference) from 20-30 min were calculated. Binding potential ( $BP_{ND}$ ) was calculated in the pancreas using SRTM. In the brain, substantia nigra (SN), caudate, putamen ROIs were defined from a brain atlas(22) coregistered to the image (30-60 min), and SUV and SUVR (cerebellum as reference) were determined. Using SUVR-1 as a measure of specific binding, percent reduction in specific pancreatic and brain binding due to the blocking drugs were determined.

To confirm the use of SUVR-1 in blocking studies, we used brain modeling methods in a second NHP (age:17y; weight:14.5kg) with baseline and blocking brain scans on the Focus 220 with only L-741,626, using the same timing and doses as above. As, in previous studies, TACs were generated for brain ROIs,  $BP_{ND}$  was calculated using SRTM2(22–24), and regional occupancy was calculated.

## RESULTS

We identified six potentially useful radioligands targeting four different receptor sites:  $^{11}\text{C}$ -raclopride,  $^{11}\text{C}$ -FLB457, and  $^{11}\text{C}$ -(+)-PHNO ( $\text{D}_2/\text{D}_3$ -receptors),  $^{11}\text{C}$ -DASB (serotonin transporter),  $^{11}\text{C}$ -AS247190 (11 $\beta$ -hydroxysteroid dehydrogenase type 1 (HSD1) enzyme inhibitor)(25) and  $^{11}\text{C}$ -UCB-J (synaptic vesicle protein 2A)(26,27). Relative gene expression of these targets are provided in Table 2. Initially, for  $\beta$ -cell gene expression screening, only the  $\text{D}_2$ -receptor gene was used to identify potential dopaminergic ligands due to the fact that all  $\text{D}_2/\text{D}_3$ -radioligands ( $^{11}\text{C}$ -raclopride,  $^{11}\text{C}$ -FLB457, and  $^{11}\text{C}$ -(+)-PHNO) target  $\text{D}_2$ -receptors to some extent, although with varying affinities for each receptor.  $^{11}\text{C}$ -raclopride and  $^{11}\text{C}$ -FLB457 are both receptor antagonists; however,  $^{11}\text{C}$ -raclopride(28) has lower affinity than  $^{11}\text{C}$ -FLB457(29).  $^{11}\text{C}$ -(+)-PHNO is an agonist with 25-50-fold higher affinity for  $\text{D}_3$ -receptors(22). Retrospective analysis after completion of PET scans to provide insight into differences between the dopaminergic radioligands included the  $\text{D}_3$ -receptor gene and the addition of the ‘Human Primary Beta Cell’ column (Table 2).

$^{11}\text{C}$ -(+)-PHNO was the only dopaminergic radioligand to demonstrate sustained uptake in the pancreas with high contrast to the kidneys, liver, and spleen, based on SUV images (20-30 minutes) and TACs (0-30 minutes). Representative PET images (Fig. 1) and TACs (Fig. 2) of the three  $\text{D}_2/\text{D}_3$ -radioligands demonstrated the apparent superiority of  $^{11}\text{C}$ -(+)-PHNO.

Low pancreas SUV and SUVR were seen in all other radioligands compared to  $^{11}\text{C}$ -(+)-PHNO (Table 3) as seen in representative PET images (Supplemental Fig. 1) and TACs (Supplemental Fig. 2). TACs (0-90 min) showed no contrast in the pancreas compared to reference organ (spleen) beyond 30 minutes for any radioligand.

$^{11}\text{C}$ - $(+)$ -PHNO pancreas SUV was  $13.8 \pm 1.7$  in HCs. A 71% reduction (SUV:4.0) was seen in the T1DM subject with undetectable C-peptide levels. In a T1DM subject with fasting C-peptide level of 0.38 ng/mL, a 20% reduction (SUV:11.0) was seen (Fig. 3; Table 4). Comparisons between TACs of the C-peptide deficient T1DM subject demonstrated substantially reduced uptake and contrast to background organs compared to the HCs (Fig. 4). SUV in other abdominal organs did not show differences between HC and T1DM (Table 5), suggesting that the  $^{11}\text{C}$ - $(+)$ -PHNO SUV differences are specific to changes in the pancreas.

Assessing the  $D_2$  and  $D_3$  components of  $^{11}\text{C}$ - $(+)$ -PHNO specific binding, SUVR-1 and  $BP_{ND}$  of  $^{11}\text{C}$ - $(+)$ -PHNO in NHP was reduced by a  $D_3$ -receptor antagonist in pancreas, SN, putamen, and caudate (Table 5; Supplemental Fig. 3). SUVR-1 and  $BP_{ND}$  for the  $D_2$ -receptor antagonist demonstrated a smaller reduction compared to the  $D_3$ -receptor antagonist in the pancreas and SN, and larger reductions in the putamen and caudate (Table 5). Using a brain-only study,  $BP_{ND}$  demonstrated similar reductions in the SN, putamen, and caudate as SUVR-1 in the previous  $D_2$ -antagonist multi-organ scan (Table 5; Supplemental Fig. 4), suggesting that SUVR-1 is a valid measure for assessing blockade.

The SN can be considered  $\sim 100\%$   $D_3$ -selective, and the putamen and caudate  $\sim 100\%$   $D_2$ -selective. Since the pancreas blocking percentages fell between the values for these regions, this suggests that  $^{11}\text{C}$ -PHNO binds to both  $D_2$  and  $D_3$  in the pancreas.

## DISCUSSION

We identified six radioligands through use of a  $\beta$ -cell gene atlas that were subsequently screened using PET/CT in HCs for high pancreas uptake and high contrast to background abdominal organs, similar to a previous study(12). The  $D_3$ -preferring radioligand  $^{11}\text{C}$ - $(+)$ -PHNO showed the best potential as a BCM-imaging agent, based on high pancreatic uptake in HCs, lower uptake in T1DM subjects, and demonstrable specific binding with NHP blocking studies.

Of the six radioligands studied, three,  $^{11}\text{C}$ -UCB-J (Synaptic vesicle protein 2A),  $^{11}\text{C}$ -DASB (serotonin transporter), and  $^{11}\text{C}$ -AS2471907 ( $11\beta$ -HSD1 enzyme inhibitor), did not demonstrate high

pancreas signal and/or contrast to background abdominal organs (Table 3). Synaptic vesicle proteins are associated with insulin-containing granules in neuroendocrine cells(30,31); however, evoked basal hormone release was attenuated more by silencing SV2C than SV2A in neuroendocrine cells, possibly explaining low SV2A signal(31). The main mechanism of 11 $\beta$ -HSD1 inhibition is lowering intracellular cortisol concentrations in liver and adipose tissue, and liver uptake was >25 times that of the pancreas, making  $^{11}\text{C}$ -AS2471907 undesirable for BCM imaging(32). Serotonin mechanisms have been implicated in the endocrine pancreas(10,33); however, given low uptake and contrast in the pancreas,  $^{11}\text{C}$ -DASB may not be a suitable BCM imaging agent.

In agreement with studies suggesting the feasibility of targeting dopamine receptors (DR) for imaging BCM(15,16,19), promising results were obtained for one of the three DR radioligands.  $^{11}\text{C}$ -(+)-PHNO demonstrated the greatest uptake and contrast compared to background organs in HCs. In contrast, a large reduction in SUV (71%) in the pancreas of a subject with T1DM without detectable C-peptide (Table 4) suggests possible specific binding of  $^{11}\text{C}$ -(+)-PHNO to islet  $\beta$ -cells. Intriguingly, a T1DM subject with detectable levels of insulin production had higher pancreas SUV than the first T1DM subject (Table 3), suggestive of intermediate BCM levels.

Using the three dopaminergic radioligands in our study, we can indirectly infer mechanisms of both D<sub>2</sub>- and D<sub>3</sub>-receptors. Based on preliminary success with D<sub>2</sub>-receptor radioligands to differentiate healthy and diabetic rats(15,16), and the  $\beta$ -cell gene atlas data (Table 2), D<sub>2</sub>-receptors may exist throughout the endocrine and exocrine pancreas. D<sub>2</sub>-receptors, as measured by  $^{11}\text{C}$ -(+)-PHNO, may not be directly or linearly correlated with  $\beta$ -cells; therefore, information obtained by this imaging technique should be viewed with caution. Further study is required to assess whether reduced D<sub>3</sub>-receptors in T1DM are specific to human  $\beta$ -cells.

$^{11}\text{C}$ -raclopride and  $^{11}\text{C}$ -FLB457 are both antagonists, and thus have equal affinity for high and low affinity receptor sites;  $^{11}\text{C}$ -FLB457 has higher affinity(29,34).  $^{11}\text{C}$ -(+)-PHNO is an agonist that binds to D<sub>2</sub>- and D<sub>3</sub>-receptors with a 25-50-fold higher affinity for D<sub>3</sub>-receptors. Quelch, et al, reported higher specific binding with [ $^3\text{H}$ ]-(+)PHNO versus [ $^3\text{H}$ ]Raclopride in microsomal but not extracellular or cytosolic tissue

in the pig striatum(35). Similar D<sub>2/3</sub>-receptor internalization may occur in the pancreas, which may explain the higher binding of <sup>11</sup>C-(+)-PHNO compared to <sup>11</sup>C-raclopride or <sup>11</sup>C-FLB457.

To assess the D<sub>2</sub>- and D<sub>3</sub>-components of pancreatic <sup>11</sup>C-(+)-PHNO binding, we performed blocking experiments in NHP. The brain occupancy data for the D<sub>3</sub>-antagonist agreed well with previous <sup>11</sup>C-(+)-PHNO data(36). For each blocking study (Table 5), using the receptor occupancy values in pancreas ( $r_{\text{panc}}$ ), putamen ( $r_{\text{put}}$ ), and SN ( $r_{\text{SN}}$ ), and assuming that SN and putamen are 100% D<sub>3</sub>- and D<sub>2</sub>-selective, respectively, we can estimate the fraction of D<sub>3</sub> ( $f_{\text{D}3}$ ) and D<sub>2</sub> ( $1-f_{\text{D}3}$ ) binding in the pancreas (See Supplemental Data for derivation of equation):

$$f_{\text{D}3} = \frac{r_{\text{panc}} - r_{\text{put}}}{r_{\text{SN}} - r_{\text{put}}} \quad (1)$$

In the D<sub>2</sub>-antagonist blocking study,  $f_{\text{D}3}$  is 0.77 using SUVR-1 or  $BP_{\text{ND}}$  and in the D<sub>3</sub>-blocking study,  $f_{\text{D}3}$  is 0.58 (SUVR-1) or 0.43 ( $BP_{\text{ND}}$ ). Averaging suggests that specific binding in the pancreas is ~two-thirds D<sub>3</sub> and one-third D<sub>2</sub>. Note that since specific binding measurements at tracer levels represent  $B_{\text{max}}/K_d$ , not  $B_{\text{max}}$ , this does not imply that two-thirds of the D<sub>2/3</sub>-receptors are D<sub>3</sub>. Rather, if the relative D<sub>2</sub>/D<sub>3</sub> affinities for <sup>11</sup>C-(+)-PHNO in the pancreas are the same as those in the brain, i.e., a 25-50-fold higher affinity for D<sub>3</sub> (22), then the  $B_{\text{max}}$  for D<sub>2</sub> is in fact much higher than that of D<sub>3</sub>.

The connection between dopaminergic activity and the endocrine pancreas has been known for 40 years(37,38). It is believed that circulating dopamine is generally below levels needed to activate peripheral dopamine receptors(39). One current theory proposes that circulating L-DOPA (dopamine precursor) is taken up by β-cells, converted to dopamine, and co-secreted with insulin as an autocrine signal by binding to dopamine receptors on the surface of β-cells(19). Dopamine antagonists have been shown to cause hyperinsulinemia in normal subjects and are associated with diabetes in psychiatric patients, vs. agonists such as bromocriptine, which improved glycemic control(40). Interestingly, L-DOPA, a common treatment in Parkinson's disease, has demonstrated reduced insulin secretion in such patients and mice (40). Combined, this evidence suggests dopamine may be an integral part of the endocrine pancreas.

Several studies have attempted to elucidate more specific mechanisms of DRs in the endocrine pancreas. *In vitro* studies using mouse islet cells have indicated that a D<sub>3</sub>-receptor antagonist increases

insulin secretion, suggesting that dopamine binding to the D<sub>3</sub>-receptor inhibits insulin secretion(18). In contrast, Chen, et al, found no evidence of pancreatic D<sub>3</sub>-receptors in rats using Western blot and immunofluorescence techniques, and concluded D<sub>1</sub>-receptors were colocalized with insulin staining in rat Islet cells(41). Additional studies have indicated the D<sub>2</sub>-receptor may be involved in insulin secretion inhibition(42–45). Several other studies have demonstrated inhibitory actions of dopamine on insulin release in preclinical models, but did not assess whether specific receptors were responsible for such actions(37,46–49). It is important to note that the structure and function of proteins may differ between species such as mouse, rat, and *in vitro* cultures of insulinoma cell lines, such as INS-1 cells. The human β-cell gene expression atlas we used demonstrated a specificity of the D<sub>3</sub>-receptor gene to β-cells and lack of expression in the exocrine and other endocrine cells in the islets of Langerhans (Table 2)(20). Further studies are warranted to determine the specificity of different DR subtypes in the endocrine pancreas and β-cells. However, from this evidence and the large reduction seen in the T1DM subject with undetectable C-peptide, we hypothesize that high affinity D<sub>3</sub>-receptors may be specific to the endocrine pancreas and perhaps to β-cells.

Several potential limitations in the current study must be assessed. The use of spleen as a reference region has been examined for the VMAT2 tracer <sup>18</sup>F-FP-(+)-DTBZ(13) and we used SUVR in the current study. A number of issues must be evaluated to validate this choice. First, presence of D<sub>2</sub>/D<sub>3</sub>-receptors in the spleen must be assessed; a preliminary study has demonstrated that all five dopamine receptor subtypes, along with VMAT1 and VMAT2, are present to some extent in the spleen(50). In NHP blocking studies, we saw 37% and 13% reductions in spleen SUV during D<sub>2</sub>- and D<sub>3</sub>-antagonist studies, respectively; however, no differences were seen between HC and T1DM subjects in spleen SUV. Second, it remains to be validated if nondisplaceable binding in the spleen is equal to the pancreas, or if a scale-factor correction is needed, as with the VMAT2 tracer(13). Further, radiolabeled metabolites may accumulate in the spleen, therefore; we focused on early data (20-30min) for the patient comparisons, to maximize specific binding while simultaneously minimizing potential biases due to radiolabeled metabolites. Arterial sampling of HC and T1DM subjects should be performed to characterize <sup>11</sup>C-(+)-PHNO metabolites and assess whether

there are between-group differences that may affect interpretation of results, similar to a previous study with enantiomers of <sup>18</sup>F-FP-DTBZ(13).

## **CONCLUSION**

We have examined 6 PET brain radioligands in the pancreas in both HC and T1DM subjects and have demonstrated that <sup>11</sup>C-(+)-PHNO, a D<sub>3</sub>-preferring receptor agonist, may be a potential marker of BCM. NHP blocking studies suggest that ~two-thirds of pancreatic binding originates from D<sub>3</sub>-receptors. Further *in vitro* and *in vivo* studies to establish D<sub>3</sub>-receptor specificity to β-cells are warranted to develop <sup>11</sup>C-(+)-PHNO as a candidate for clinical measurement of BCM.

## **ACKNOWLEDGEMENTS**

The authors appreciate the excellent technical assistance of the Yale PET Center staff. This study was supported by the NIH grant 1DP3DK104092-01 and also made possible by 1S10OD010322-01 and by CTSA Grant Number UL1 TR000142 from the National Center for Advancing Translational Sciences (NCATS), a component of the NIH. Its contents are solely the responsibility of the authors and do not necessarily represent the official view of the NIH.

## REFERENCES

1. Steele C, Hagopian W, Gitelman S, et al. Insulin secretion in type 1 diabetes. *Diabetes*. 2004;53:426-433.
2. Meier JJ, Menge B, Breuer TGK, et al. Functional assessment of pancreatic  $\beta$ -cell area in humans. *Diabetes*. 2009;58:1595-1603.
3. Meier JJ, Bonadonna RC. Role of reduced  $\beta$ -cell mass versus impaired  $\beta$ -cell function in the pathogenesis of type 2 diabetes. *Diabetes Care*. 2013;36.
4. Weir GC, Bonner-Weir S. Sleeping islets and the relationship between  $\beta$ -cell mass and function. *Diabetes*. 2011;60:2018-2019.
5. Weir GC, Bonner-Weir S. Islet  $\beta$ -cell mass in diabetes and how it relates to function, birth, and death. *Ann N Y Acad Sci* 2013;1281:92-105.
6. Jodal A, Schibli R, Béhé M. Targets and probes for non-invasive imaging of  $\beta$ -cells. *Eur J Nucl Med Mol Imaging*. 2017;44:712-727.
7. Goland R, Freeby M, Parsey R, et al. <sup>11</sup>C-dihydrotetrabenazine PET of the pancreas in subjects with long-standing type 1 diabetes and in healthy controls. *J Nucl Med*. 2009;50:382-389.
8. Singhal T, Ding YS, Weinzimer D, et al. Pancreatic beta-cell mass PET imaging and quantification with [<sup>11</sup>C]DTBZ and [<sup>18</sup>F]FP-(+)-DTBZ in rodent models of diabetes. *Mol Imaging Biol*. 2011;13:973-984.
9. Normandin MD, Petersen KF, Ding Y-S, et al. In vivo imaging of endogenous pancreatic  $\beta$ -cell mass in healthy and type 1 diabetic subjects using <sup>18</sup>F-Fluoropropyl-Dihydrotetrabenazine and PET. *J Nucl Med*. 2012;53:908-916.
10. Eriksson O, Espes D, Selvaraju RK, et al. Positron emission tomography ligand [<sup>11</sup>C]5-Hydroxy-Tryptophan can be used as a surrogate marker for the human endocrine pancreas. *Diabetes*. 2014;63:3428-3437.
11. Freeby MJ, Kringas P, Goland RS, et al. Cross-sectional and test-retest characterization of PET with [<sup>18</sup>F]FP-(+)-DTBZ for  $\beta$ -Cell mass estimates in diabetes. *Mol Imaging Biol*. 2016;18:292-301.
12. Karlsson F, Antonodimitrakis PC, Eriksson O. Systematic screening of imaging biomarkers for the Islets of Langerhans, among clinically available positron emission tomography tracers. *Nucl Med Biol*. 2015;42(10):762-769.
13. Naganawa M, Lin S-F, Lim K, et al. Evaluation of pancreatic VMAT2 binding with active and inactive enantiomers of (<sup>18</sup>F)FP-DTBZ in baboons. *Nucl Med Biol*. 2016;43:743-751.
14. Carlblom L, Espes D, Lubberink M, et al. [<sup>11</sup>C]5-hydroxy-tryptophan PET for assessment of islet mass during progression of type 2 diabetes. *Diabetes*. 2017;1:1-25.
15. Garcia A, Venugopal A, Pan M-L, Mukherjee J. Imaging pancreas in healthy and diabetic rodent model using [<sup>18</sup>F]Fallypride positron emission tomography/computed tomography. *Diabetes Technol Ther*. 2014;16:640-643.
16. Willekens SMA, Van Der Kroon I, Joosten L, et al. SPECT of transplanted islets of langerhans by dopamine 2 Receptor targeting in a rat model. *Mol Pharm*. 2016;13:85-91.
17. Saisho Y, Harris PE, Butler AE, et al. Relationship between pancreatic vesicular monoamine transporter 2 (VMAT2) and insulin expression in human pancreas. *J Mol Histol*. 2008;39:543-551.
18. Ustione A, Piston DW. Dopamine synthesis and D3-Receptor activation in pancreatic  $\beta$ -cells regulates insulin secretion and intracellular  $[Ca^{2+}]$  oscillations. *Mol Endocrinol*. 2012;26:1928-

1940.

19. Ustione A, Piston DW, Harris PE. Minireview: dopaminergic regulation of insulin secretion from the pancreatic islet. *Mol Endocrinol*. 2013;27:1198-207.
20. Kutlu B, Burdick D, Baxter D, et al. Detailed transcriptome atlas of the pancreatic beta-cell. *BMC Med Genomics*. 2009;2:3.
21. Ren S, Jin X, Chan C, et al. Data-driven respiratory motion estimation and correction using TOF PET list-mode centroid of distribution. *Phys Med Biol*. 2017;62:4741-4755.
22. Gallezot JD, Beaver JD, Gunn RN, et al. Affinity and selectivity of [<sup>11</sup>C]-(+)-PHNO for the D<sub>3</sub> and D<sub>2</sub>-receptors in the rhesus monkey brain in vivo. *Synapse*. 2012;66:489-500.
23. Innis RB, Cunningham VJ, Delforge J, et al. Consensus nomenclature for in vivo imaging of reversibly binding radioligands. *J Cereb Blood Flow Metab*. 2007;27:1533-1539.
24. Wu Y, Carson RE. Noise reduction in the simplified reference tissue model for neuroreceptor functional imaging. *J Cereb Blood Flow Metab*. 2002;22:1440-1452.
25. Huang Y, Planet B, Nabulsi N, et al. First-in-human study of the 11{beta}-hydroxysteroid dehydrogenase type 1 PET tracer [<sup>11</sup>C]AS2471907. *J Nucl Med*. 2016;57:580-.
26. Nabulsi N, Mercier J, Holden D, et al. Synthesis and preclinical evaluation of <sup>11</sup>C-UCB-J as a PET tracer for imaging the synaptic vesicle glycoprotein 2A in the brain. *J Nucl Med*. 2016;777-785.
27. Finnema SJ, Nabulsi NB, Eid T, et al. Imaging synaptic density in the living human brain. *Sci Transl Med*. 2016;8:348ra96-348ra96.
28. Farde L, Eriksson L, Blomquist G, Halldin C. Kinetic analysis of central [<sup>11</sup>C]raclopride binding to D<sub>2</sub>-dopamine receptors studied by PET--a comparison to the equilibrium analysis. *J Cereb Blood Flow Metab*. 1989;9:696-708.
29. Halldin C, Farde L, Höglberg T, et al. Carbon-11-FLB 457: a radioligand for extrastratal D<sub>2</sub> dopamine receptors. *J Nucl Med*. 1995;36:1275-1281.
30. Portela-Gomes GM, Lukinius A, Grimelius L. Synaptic vesicle protein 2, A new neuroendocrine cell marker. *Am J Pathol*. 2000;157:1299-1309.
31. Iezzi M, Theander S, Janz R, et al. SV2A and SV2C are not vesicular Ca<sup>2+</sup> transporters but control glucose-evoked granule recruitment. *J Cell Sci*. 2005;118:5647-5660.
32. Pereira CD, Azevedo I, Monteiro R, Martins MJ. 11β-Hydroxysteroid dehydrogenase type 1: relevance of its modulation in the pathophysiology of obesity, the metabolic syndrome and type 2 diabetes mellitus. *Diabetes Obes Metab*. 2012;14:869-881.
33. Eriksson O, Selvaraju RK, Johansson L, et al. Quantitative imaging of serotonergic biosynthesis and degradation in the endocrine pancreas. *J Nucl Med*. 2014;55:460-5.
34. Seeman P. Antipsychotic drugs, dopamine receptors, and schizophrenia. *Clin Neurosci Res*. 2001;1:53-60.
35. Quelch DR, Withey SL, Nutt DJ, et al. The influence of different cellular environments on PET radioligand binding: an application to D<sub>2</sub>/D<sub>3</sub>-dopamine receptor imaging. *Neuropharmacology*. 2014;85:305-313.
36. Rabiner E, Slifstein M, Nobrega J, et al. In vivo quantification of regional dopamine-D<sub>3</sub> receptor binding potential of (+)-PHNO: Studies in non-human primates and transgenic mice. *Synapse*. 2009;63:782-793.
37. Ericson LE, Håkanson R, Lundquist I. Accumulation of dopamine in mouse pancreatic β-cells

- following injection of L-DOPA Localization to secretory granules and inhibition of insulin secretion. *Diabetologia* 1977;13:117-124.
38. Leblanc H, Lachelin GCL, Yen SSC, et al. The effect of dopamine infusion on insulin and glucagon secretion in man. *J Clin Endocrinol Metab*. 1977;44(1):196-198.
  39. Goldstein DS, Eisenhofer G, Kopin IJ. Sources and significance of plasma levels of catechols and their metabolites in humans. *J Pharmacol Exp Ther*. 2003;305:800-811.
  40. Lopez Vicchi F, Luque GM, Brie B, et al. Dopaminergic drugs in type 2 diabetes and glucose homeostasis. *Pharmacol Res*. 2015;109:74-80.
  41. Chen Y, Hong F, Chen H, et al. Distinctive expression and cellular distribution of dopamine receptors in the pancreatic islets of rats. *Cell Tissue Res*. 2014;597-606.
  42. Rubi B, Ljubicic S, Pournourmohammadi S, et al. Dopamine D2-like receptors are expressed in pancreatic  $\beta$ -cells and mediate inhibition of insulin secretion. *J Biol Chem*. 2005;280:36824-36832.
  43. García-Tornadú I, Ornstein AM, Chamson-Reig A, et al. Disruption of the dopamine D2-receptor impairs insulin secretion and causes glucose intolerance. *Endocrinology*. 2010;151:1441-1450.
  44. Simpson N, Maffei A, Freeby M, et al. Dopamine-mediated autocrine inhibitory circuit regulating human insulin secretion in vitro. *Mol Endocrinol*. 2012;26:1-16.
  45. Sakano D, Choi S, Kataoka M, et al. Dopamine D2 receptor-mediated regulation of pancreatic  $\beta$ -cell mass. *Stem Cell Reports*. 2016;7:95-109.
  46. Barrado MJG, Osma MCI, Blanco EJ, et al. Dopamine modulates insulin release and is involved in the survival of rat pancreatic  $\beta$ -cells. *PLoS One*. 2015;10:1-16.
  47. Maffei A, Segal AM, Alvarez-Perez JC, et al. Anti-incretin, anti-proliferative action of dopamine on  $\beta$ -cells. *Mol Endocrinol*. 2015;29:542-57.
  48. Mezey E, Eisenhofer G, Harta G, et al. A novel nonneuronal catecholaminergic system: exocrine pancreas synthesizes and releases dopamine. *Proc Natl Acad Sci*. 1996;93:10377-10382.
  49. Miller RE. Pancreatic neuroendocrinology: peripheral neural mechanisms in the regulation of the Islets of Langerhans. *Endocr Rev*. 1981;2:471-494.
  50. Mignini F, Tomassoni D, Traini E, Amenta F. Dopamine, vesicular transporters and dopamine receptor expression and localization in rat thymus and spleen. *J Neuroimmunol*. 2009;206:5-13.

## TABLES

**Table 1** Injected doses and mass (min-max) for radioligands and respective targets in human studies. Two subjects (1M/1F) were scanned for each radioligand with the exception of <sup>11</sup>C-(+)-PHNO (n=4).

Radioactive Ligand	Radioactive Ligand Target	Injected Dose (MBq)	Injected Mass (µg)
<sup>11</sup> C-(+)-PHNO	D <sub>2</sub> /D <sub>3</sub> -receptors	209-351	1.63-2.30
<sup>11</sup> C-FLB457	D <sub>2</sub> /D <sub>3</sub> -receptors	326-344	0.59-0.60
<sup>11</sup> C-Raclopride	D <sub>2</sub> /D <sub>3</sub> -receptors	272-346	0.45-3.27
<sup>11</sup> C-DASB	Serotonin transporter	166-359	0.25-0.61
<sup>11</sup> C-AS2471907	11β-HSD1 enzyme inhibitor	208-214	2.75-3.00
<sup>11</sup> C-UCB-J	Synaptic vesicle protein 2A	46-322	1.00-1.49

**Table 2** Radioligand target relative gene expression with rankings of 0-100 gathered from a beta cell gene atlas.(20) Expression group rankings: none (0-25), low (25-50), moderate (50-75), enriched (75-100). DRD2—dopamine receptor 2, DRD3—dopamine receptor 3, SLC6A4—serotonin transporter, HSD11B1—11β-hydroxysteroid dehydrogenase type 1 enzyme inhibitor, SV2A—synaptic vesicle protein 2A. (\*)Retrospective analysis for relative gene expression was examined after completion of PET scans to provide insight into differences of pancreas uptake between the three D<sub>2</sub>/D<sub>3</sub>-receptor radioligands (<sup>11</sup>C-raclopride, <sup>11</sup>C-FLB457, and <sup>11</sup>C-(+)-PHNO).

Gene Expression				
Radioactive Ligand(s)	Gene	Human Exocrine Pancreas	Human Pancreatic Islets	Human Primary Beta Cells*
<sup>11</sup> C-(+)-PHNO <sup>11</sup> C-FLB457 <sup>11</sup> C-Raclopride	DRD2	63	55	74*
	DRD3*	1*	4*	69*
<sup>11</sup> C-DASB	SLC6A4	59	69	54*
<sup>11</sup> C-AS2471907	HSD11B1	44	75	48*
<sup>11</sup> C-UCB-J	SV2A	16	72	86*

**Table 3** Mean±standard deviation pancreatic SUV (20-30 minutes) of each radioligand in healthy controls (SUVR, spleen reference).

<b>Radioligand</b>	<b>Pancreas (SUV)</b>	<b>Pancreas/Spleen (SUVR)</b>
<sup>11</sup> C-(+)-PHNO	13.8±1.7	7.1±0.4
<sup>11</sup> C-FLB457	3.0±0.8	0.9±0.0
<sup>11</sup> C-Raclopride	2.2±0.5	1.4±0.0
<sup>11</sup> C-DASB	4.0±0.6	0.7±0.1
<sup>11</sup> C-AS2471907	0.6±0.1	0.4±0.1
<sup>11</sup> C-UCB-J	1.6±0.4	1.7±0.3

**Table 4** Mean±standard deviation SUV (20-30 minutes) of <sup>11</sup>C-(+)-PHNO in pancreas, spleen, kidneys and liver. (\*)undetectable C-peptide T1DM subject. (^)detectable C-peptide T1DM subject

<sup>11</sup> C-(+)-PHNO	Pancreas/Spleen (SUVR)	Pancreas (SUV)	Spleen (SUV)	Kidneys (SUV)	Liver (SUV)
<b>Healthy Controls (n=2)</b>	7.1±0.4	13.8±1.7	2.0±0.3	5.9±3.0	7.2±1.7
<b>T1DM (n=2)</b>	2.1*	4.4^	4.0* 11.0^	2.2±0.4	5.0±0.4 7.8±1.6

**Table 5** SUVR-1 and  $BP_{ND}$  in baseline and blocking scans, and percent reduction from baseline in pancreas and brain regions in non-human primates with  $^{11}\text{C}-(+)$ -PHNO.  $BP_{ND}$  calculated using SRTM for pancreas (spleen reference) and SRTM2 for brain (cerebellum reference). (^)Dynamic data not available. Data presented as Baseline values/Blocking values/Percent reduction.

Antagonist	Measure	Pancreas	Substantia Nigra	Putamen	Caudate
<b>D<sub>3</sub></b>	<b>SUVR-1</b>	2.8/1.2/57%	2.8/0.3/89%	4.7/4.1/13%	3.7/2.9/22%
	<b>BP<sub>ND</sub></b>	1.5/0.8/46%	^	^	^
<b>D<sub>2</sub></b>	<b>SUVR-1</b>	1.6/1.0/38%	4.0/3.0/25%	5.8/1.1/81%	5.2/1.4/73%
	<b>BP<sub>ND</sub></b>	0.8/0.5/38%	^	^	^
<b>D<sub>2</sub></b>	<b>BP<sub>ND</sub></b>	^	3.5/2.7/23%	4.3/0.9/79%	4.3/0.9/79%

## FIGURES

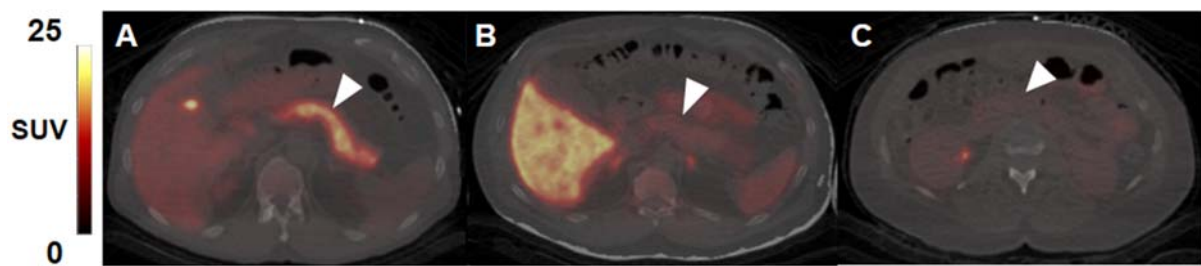


**Figure 1** Representative axial slices of PET/CT overlay of pancreas uptake (white arrows) for each dopaminergic radioligand **A)**  $^{11}\text{C}$ - $(+)$ -PHNO **B)**  $^{11}\text{C}$ -FLB457 and **C)**  $^{11}\text{C}$ -Raclopride. All SUV images summed from 20-30 minutes.

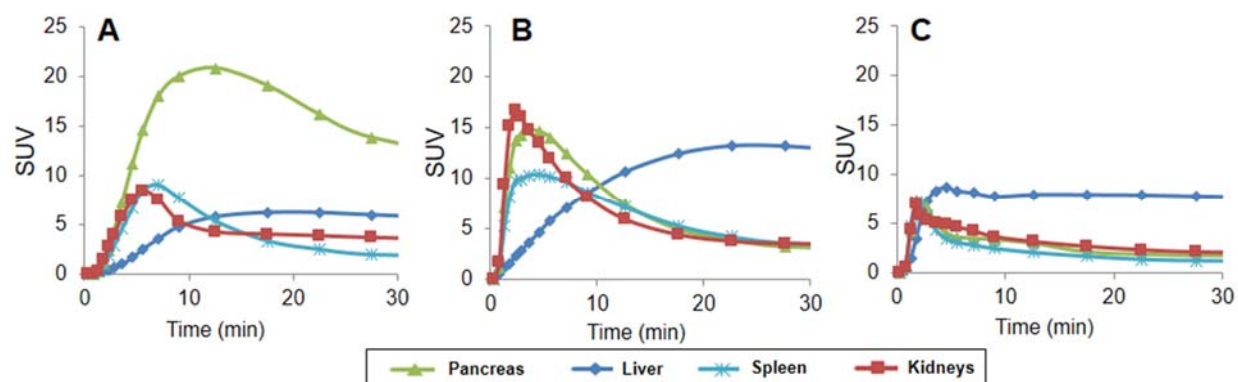


**Figure 2** Mean time activity curves of pancreas, liver, spleen and kidneys of two healthy controls for each dopaminergic radioligand **A)**  $^{11}\text{C}$ - $(+)$ -PHNO **B)**  $^{11}\text{C}$ -FLB457 and **C)**  $^{11}\text{C}$ -Raclopride.

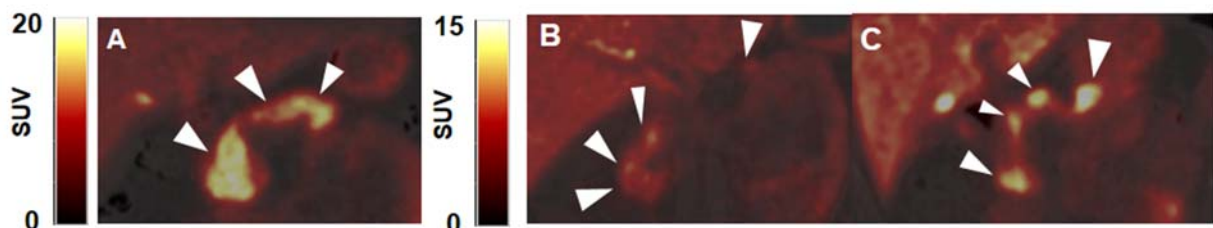


**Figure 3** Representative coronal PET/CT images of  $^{11}\text{C}$ - $(+)$ -PHNO in pancreas (white arrows) for **A)** healthy control **B)** C-peptide deficient T1DM subject **C)** T1DM subject with detectable C-peptide All SUV images summed from 20-30 minutes. **A)** SUV scale 0-20 **B-C)** SUV scale 0-15.

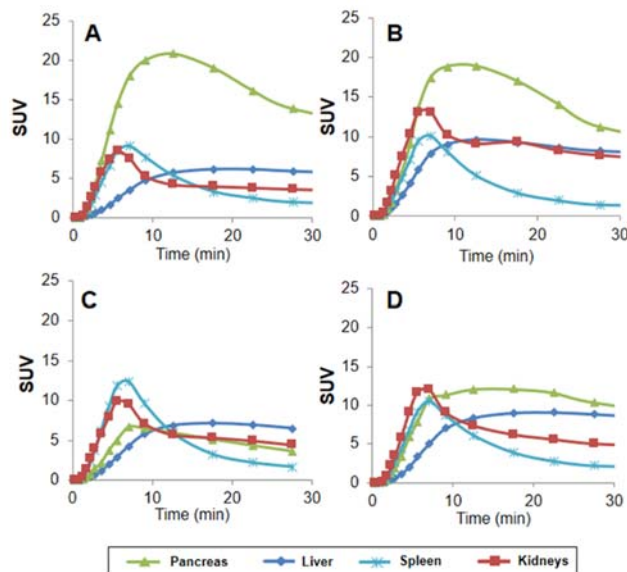
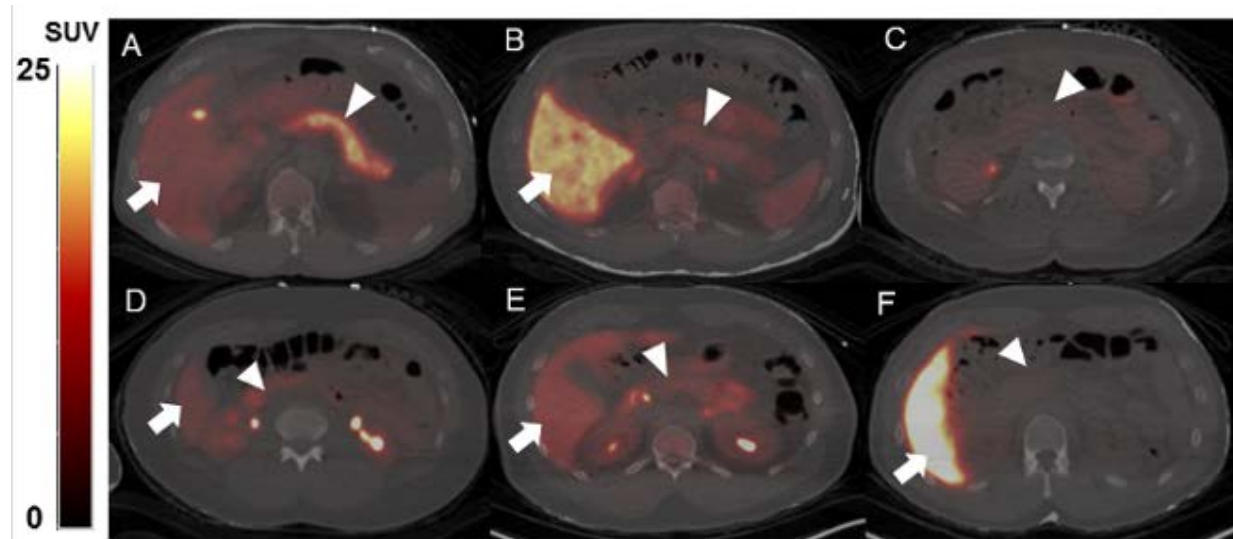
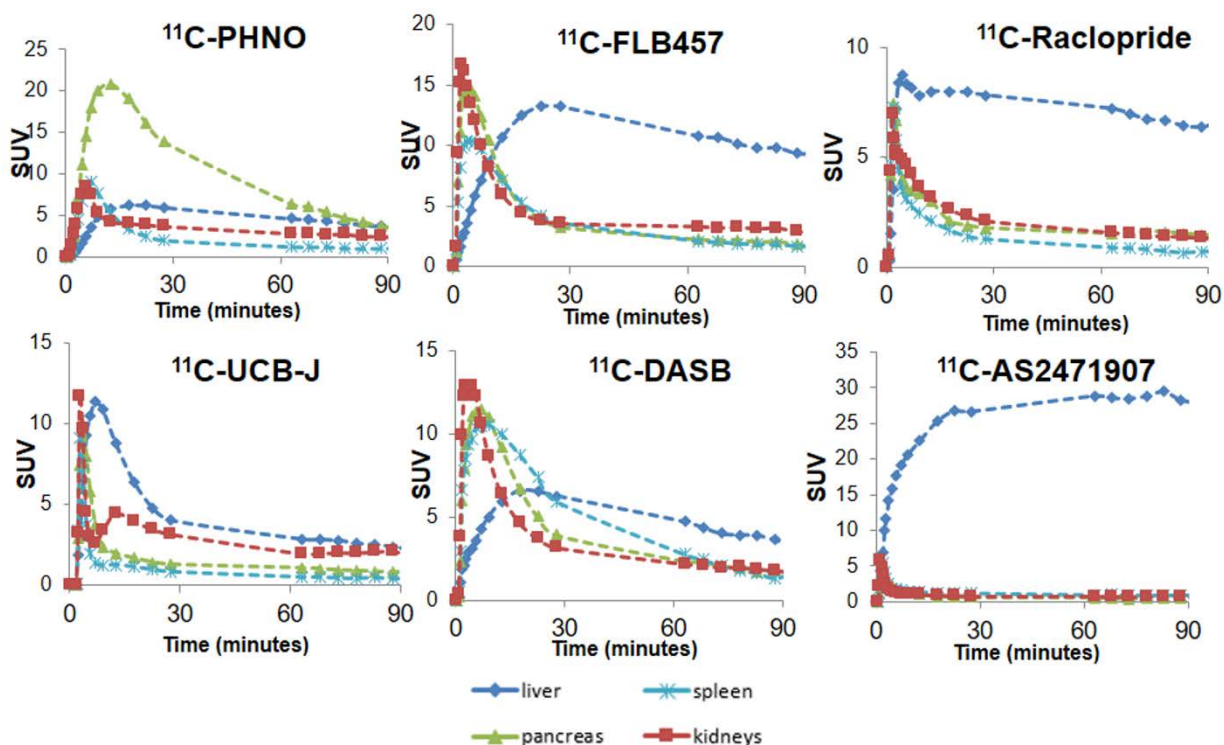


**Figure 4**  $^{11}\text{C}$ -(-)-PHNO time activity curves of pancreas, liver, spleen and kidneys for **A, B)** healthy controls; **C)** C-peptide deficient T1DM; **D)** T1DM subject with detectable C-peptide.

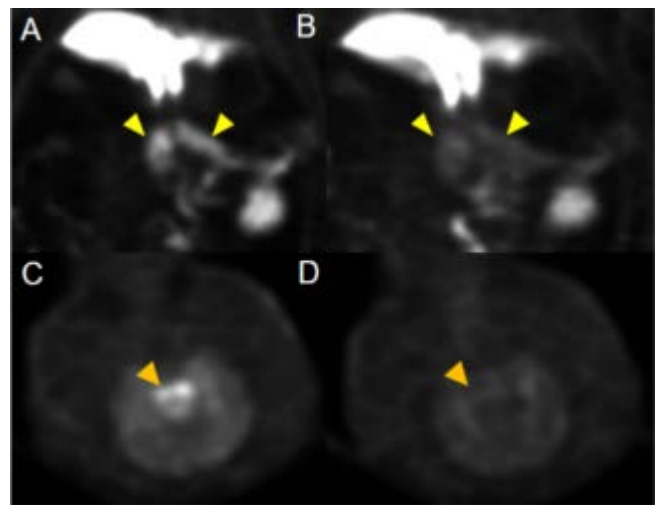
## SUPPLEMENTAL FIGURES



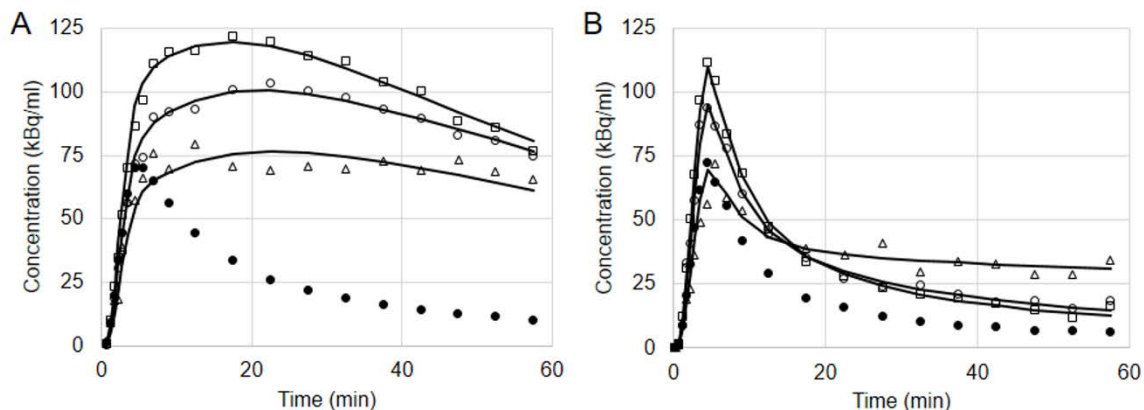
**Supplemental Figure 1** Representative axial slices of pancreas uptake (white arrowhead) for **A**)  $^{11}\text{C}$ -(-)-PHNO ( $\text{D}_2/\text{D}_3$  receptors) **B**)  $^{11}\text{C}$ -FLB457 ( $\text{D}_2/\text{D}_3$  receptors) **C**)  $^{11}\text{C}$ -Raclopride ( $\text{D}_2/\text{D}_3$  receptors) **D**)  $^{11}\text{C}$ -UCB-J (Synaptic Vesicle Protein 2A) **E**)  $^{11}\text{C}$ -DASB (Serotonin Transporter) and **F**)  $^{11}\text{C}$ -AS2471907 ( $11\beta$ -hydroxysteroid dehydrogenase type 1 enzyme inhibitor). All SUV images summed from 20-30 minutes. Liver marked with white arrow for reference when in the field-of-view.



**Supplemental Figure 2** Representative time activity curves of pancreas, liver, spleen and kidneys for all radioligands for the 90-min scan duration. Gap from 30-60 minutes represents the 30-minute whole body acquisition (2 passes, 120s per bed position). Note: different SUV scales for each graph



**Supplemental Figure 3** Representative images of a non-human primate  $^{11}\text{C}$ -(-)-PHNO scan **A**) baseline scan (20-30 min) of pancreas (yellow arrows) **B**) blocking scan following 1 mg/kg of the  $\text{D}_3$ -antagonist SB277011-A. **C**) baseline scan (30-60 min) at the level of the substantia nigra (orange arrow) **D**) blocking scan following same antagonist dose.



**Supplemental Figure 4** Regional time-activity curves from  $^{11}\text{C}$ -(-)-PHNO **A**) baseline and **B**) blocking (1.0mg/kg  $\text{D}_2$ -selective antagonist L-741,626) scans in non-human primate. Example time-activity curves obtained in the cerebellum (solid circles), caudate (open circles), putamen (open squares) and substantia nigra (open triangles). The solid lines correspond to SRTM2 curve fits using cerebellum as reference region.

### Derivation of Equation to Estimate Fraction of D<sub>2</sub>- and D<sub>3</sub>-receptor Binding in Pancreas

The following derivation provides an equation to estimate the fraction of D<sub>2</sub>- and D<sub>3</sub>-receptor binding in the pancreas, using <sup>11</sup>C-(+)-PHNO non-human primate baseline and blocking PET studies. Let  $f_{D3}$  and  $f_{D2}$  be the fraction of the binding potential at D<sub>3</sub> and D<sub>2</sub> sites, respectively.

$$f_{D3} + f_{D2} = 1 \quad (\text{S1})$$

If  $BP_{ND,base}$  is the binding potential at baseline, then  $f_{D3}BP_{ND,base}$  is the binding potential due to D<sub>3</sub> binding and  $f_{D2}BP_{ND,base}$  is the binding potential due to D<sub>2</sub> binding. During a blocking study, let  $r_{D3}$  and  $r_{D2}$  be the receptor occupancy at D<sub>3</sub> and D<sub>2</sub> sites, respectively. Then, the binding potential during the blocking study,  $BP_{ND,block}$  is:

$$BP_{ND,block} = f_{D3}(1 - r_{D3})BP_{ND,base} + f_{D2}(1 - r_{D2})BP_{ND,base} \quad (\text{S2})$$

Dividing by  $BP_{ND,base}$

$$\frac{BP_{ND,block}}{BP_{ND,base}} = f_{D3} - f_{D3}r_{D3} + f_{D2} - f_{D2}r_{D2} \quad (\text{S3})$$

Using relationship described in (S1), above:

$$\frac{BP_{ND,block}}{BP_{ND,base}} = 1 - f_{D3}r_{D3} - f_{D2}r_{D2} \quad (\text{S4})$$

Approximating  $BP_{ND}$  with (SUVR-1) (which would be exact at equilibrium);

$$\frac{SUVR_{block}-1}{SUVR_{base}-1} = 1 - f_{D3}r_{D3} - f_{D2}r_{D2} \quad (\text{S5})$$

Rearranging:

$$1 - \frac{SUVR_{block}-1}{SUVR_{base}-1} = f_{D3}r_{D3} + f_{D2}r_{D2} \quad (\text{S6})$$

Define the net occupancy in the pancreas  $r_{panc} = 1 - (SUVR_{block} - 1 / SUVR_{base} - 1)$

$$r_{panc} = f_{D3}r_{D3} + (1 - f_{D3})r_{D2} \quad (\text{S7})$$

Solve for  $f_{D3}$ :

$$f_{D3} = \frac{r_{panc} - r_{D2}}{r_{D3} - r_{D2}} \quad (\text{S8})$$

$$f_{D2} = \frac{r_{panc} - r_{D3}}{r_{D2} - r_{D3}} \quad (\text{S9})$$

Pancreas occupancy,  $r_{panc}$  is determined with either a D<sub>2</sub>- or D<sub>3</sub>-antagonist (Table 5). Brain occupancy values ( $r$ ) are chosen from known D<sub>2</sub>- or D<sub>3</sub>-receptor rich regions, i.e., putamen ( $r_{put}$ ), (~100% D<sub>2</sub>) and substantia nigra ( $r_{SN}$ ), (~100% D<sub>3</sub>), respectively (Table 5). In S9, where subscripts D<sub>2</sub> become putamen and D<sub>3</sub> becomes SN we use the assumption that 100% of the binding in the putamen is D<sub>2</sub> binding and 100% of substantia nigra binding is D<sub>3</sub>. In addition, it is assumed that antagonists have the same effect on pancreatic dopamine receptors as brain dopamine receptors. Specifically, we assume the same free drug concentrations are reached in pancreas and brain and that affinities of the drugs at D<sub>2</sub> and D<sub>3</sub> receptors

are the same in pancreas as in brain. These assumptions allow for an occupancy estimate of  $D_2$  and  $D_3$  binding in the pancreas. i.e.,

$$f_{D3} = \frac{r_{\text{panc}} - r_{\text{put}}}{r_{\text{SN}} - r_{\text{put}}} \quad (\text{S10})$$

$$f_{D2} = \frac{r_{\text{panc}} - r_{\text{SN}}}{r_{\text{put}} - r_{\text{SN}}} \quad (\text{S11})$$